1-8-2016

Pulmonary Imaging Biomarkers of Gas Trapping and Emphysema in COPD: (3)He MR Imaging and CT Parametric Response Maps

Dante P I Capaldi

Nanxi Zha

Fumin Guo

Damien Pike

David G McCormack

See next page for additional authors

Pulmonary Imaging Biomarkers of Gas Trapping and Emphysema in COPD: ^{3}He MR Imaging and CT Parametric Response Maps[1]

Dante P. I. Capaldi, BSc
Nanxi Zha, BEng
Fumin Guo, MEng
Damien Pike, BSc
David G. McCormack, MD, FRCPC
Miranda Kirby, PhD
Grace Parraga, PhD

Purpose: To directly compare magnetic resonance (MR) imaging and computed tomography (CT) parametric response map (PRM) measurements of gas trapping and emphysema in ex-smokers both with and without chronic obstructive pulmonary disease (COPD).

Materials and Methods: Participants provided written informed consent to a protocol that was approved by a local research ethics board and Health Canada and was compliant with the HIPAA (Institutional Review Board Reg. #00000940). The prospectively planned study was performed from March 2014 to December 2014 and included 58 ex-smokers (mean age, 73 years ± 9) with (n = 32; mean age, 74 years ± 7) and without (n = 26; mean age, 70 years ± 11) COPD. MR imaging (at functional residual capacity plus 1 L), CT (at full inspiration and expiration), and spirometry or plethysmography were performed during a 2-hour visit to generate ventilation defect percent (VDP), apparent diffusion coefficient (ADC), and PRM gas trapping and emphysema measurements. The relationships between pulmonary function and imaging measurements were determined with analysis of variance (ANOVA), Holm-Bonferroni corrected Pearson correlations, multivariate regression modeling, and the spatial overlap coefficient (SOC).

Results: VDP, ADC, and PRM gas trapping and emphysema (ANOVA, $P <$ .001) measurements were significantly different in healthy ex-smokers than they were in ex-smokers with COPD. In all ex-smokers, VDP was correlated with PRM gas trapping (r = 0.58, $P <$ .001) and with PRM emphysema (r = 0.68, $P <$ .001). VDP was also significantly correlated with PRM in ex-smokers with COPD (gas trapping: r = 0.47 and P = .03; emphysema: r = 0.62 and $P <$ .001) but not in healthy ex-smokers. In a multivariate model that predicted PRM gas trapping, the forced expiratory volume in 1 second normalized to the forced vital capacity (standardized coefficients [β_S] = −0.69, P = .001) and airway wall area percent (β_S = −0.22, P = .02) were significant predictors. PRM emphysema was predicted by the diffusing capacity for carbon monoxide (β_S = −0.29, P = .03) and VDP (β_S = 0.41, P = .001). Helium 3 ADC values were significantly elevated in PRM gas-trapping regions ($P <$ .001). The spatial relationship for ventilation defects was significantly greater with PRM gas trapping than with PRM emphysema in patients with mild (for gas trapping, SOC = 36% ± 28; for emphysema, SOC = 1% ± 2; P = .001) and moderate (for gas trapping, SOC = 34% ± 28; for emphysema, SOC = 7% ± 15; P = .006) COPD. For severe COPD, the spatial relationship for ventilation defects with PRM emphysema (SOC = 64% ± 30) was significantly greater than that for PRM gas trapping (SOC = 36% ± 18; P = .01).

Conclusion: In all ex-smokers, ADC values were significantly elevated in regions of PRM gas trapping, and VDP was quantitatively and spatially related to both PRM gas trapping and PRM emphysema. In patients with mild to moderate COPD, VDP was related to PRM gas trapping, whereas in patients with severe COPD, VDP correlated with both PRM gas trapping and PRM emphysema.

Online supplemental material is available for this article.

An earlier incorrect version of this article appeared online. This article was corrected on January 12, 2016.

[1] From the Imaging Research Laboratories, Robarts Research Institute, 1151 Richmond St N, London, ON, Canada N6A 5B7 (D.P.I.C., N.Z., F.G., D.P., G.P.); Department of Medical Biophysics (D.P.I.C., D.P., G.P.), Graduate Program in Biomedical Engineering (F.G., G.P.), and Division of Respirology, Department of Medicine (D.G.M.), The University of Western Ontario, London, Ont, Canada; and Heart and Lung Institute, St Paul's Hospital, Vancouver, BC, Canada (M.K.). Received July 15, 2015; revision requested August 31; revision received September 11; accepted October 5; final version accepted October 15. Supported by the Canadian Institutes of Health Research Team (grant CIF#97687, Thoracic Imaging Network of Canada), M.K. supported by the Canadian Institutes of Health Research Banting Postdoctoral Fellowship program, D.P.I.C. supported by the Natural Sciences and Engineering Research Council of Canada Doctoral Postgraduate Scholarships, and G.P. supported by a Canadian Institutes of Health Research New Investigator award. **Address correspondence to** G.P. (e-mail: *gparraga@robarts.ca*).

Chronic obstructive pulmonary disease (COPD) is characterized by persistent airflow limitation related to airway remodeling, inflammation, and emphysematous destruction (1). These pathophysiologic features can be regionally quantified by using high-resolution x-ray computed tomography (CT) measurements of the airways and parenchyma (2–5). For example, airways disease can be estimated by using CT measurements of airway wall area percent and lumen area, whereas emphysema may be estimated by using CT attenuation thresholds, such as −950 HU or the 15th percentile value from inspiratory CT (4,6). The expiratory CT attenuation-histogram threshold of −856 HU also provides a way to estimate gas trapping, reflecting the longer time constants for emptying the parenchyma via obstructed airways (7).

Recently, parametric response mapping (PRM) was used to evaluate COPD, breast cancer treatment response, and osteoporosis (8–11). In patients with COPD, coregistered inspiratory and expiratory thoracic CT can be evaluated by using well-established attenuation thresholds, resulting in the classification of healthy, emphysematous, and gas-trapping lung regions (9,12). However, the relationship of PRM-classified tissue with other established measurements of airways disease and emphysema is not well understood. Very recently, PRM phenotyping was used to differentiate among current and former smokers with and without COPD, but the clinical relevance and cause of PRM measurements of airways disease is uncertain (13).

Single photon emission computed tomography and positron emission tomography have also been used to depict pulmonary function abnormalities in patients with COPD (14,15). In addition, hyperpolarized inhaled noble gas MR imaging with helium 3 (^{3}He) and xenon 129 gases, as well as oxygen-enhanced and fluorine 19 magnetic resonance (MR) imaging, provide other ways to quantify both functional and structural pulmonary biomarkers of COPD (16–19). Hyperpolarized ^{3}He MR imaging apparent diffusion coefficients (ADCs) reflect the size of the lung acinar units. Such values are abnormally elevated in smokers with and without COPD (20,21). ^{3}He MR imaging ventilation defects may reflect both airways disease and emphysema in patients with advanced COPD, but in mild COPD and asthma, ventilation defects reflect airways disease (22,23). Despite the potential of ^{3}He MR imaging, limited

Advances in Knowledge

- In 58 ex-smokers with (n = 32) and without (n = 26) chronic obstructive pulmonary disease (COPD), ^{3}He MR imaging ventilation defect percent (VDP) was significantly correlated with inspiratory and expiratory CT parametric response map (PRM) measurements of gas trapping (r = 0.58, P < .001) and emphysema (r = 0.68, P < .001); ^{3}He apparent diffusion coefficient (ADC) values were also significantly correlated with PRM gas trapping (r = 0.55, P < .001) and PRM emphysema (r = 0.62, P < .001).
- In a significant multivariate model that predicted PRM gas trapping, the forced expiratory volume in 1 second normalized to the forced vital capacity (standardized coefficient [β_S] = −0.69, P = .001) and airway wall area percent (β_S = −0.22, P = .02) were significant predictors, whereas PRM emphysema was predicted by MR imaging VDP (β_S = 0.41, P = .001) and diffusing capacity for carbon monoxide (β_S = −0.29, P = .03).
- In all ex-smokers, spatial CT and MR imaging relationships showed that ^{3}He MR imaging ADC values were significantly elevated in regions of PRM gas trapping (P < .001).
- In patients with mild (for gas trapping, spatial overlap coefficient [SOC] = 36% ± 28; for emphysema, SOC = 1% ± 2; P = .001) and moderate (for gas trapping, SOC = 34% ± 28; for emphysema, SOC = 7% ± 15; P = .006) COPD (n = 25), ^{3}He MR imaging ventilation defects were quantitatively and spatially related to PRM gas trapping, whereas in patients with severe COPD (n = 7), MR imaging ventilation defects were quantitatively and spatially related to both PRM gas trapping and emphysema (for gas trapping, SOC = 36% ± 18; for emphysema, SOC = 64% ± 30; P = .01).

Implications for Patient Care

- In ex-smokers with mild (P = .001) and moderate (P = .006) COPD, regions of PRM gas trapping were spatially and quantitatively related to MR imaging ventilation abnormalities, whereas in patients with severe COPD, ventilation abnormalities were related to both PRM gas trapping (P = .009) and PRM emphysema (P = .01).
- While ^{3}He MR imaging is unlikely to be translated clinically, this information may be used to help better understand PRM gas trapping measurements, which may be more widely adopted for clinical phenotyping in patients with COPD.

Published online before print
10.1148/radiol.2015151484 **Content codes:** CH CT MR

Radiology 2016; 279:597–608

Abbreviations:
ADC = apparent diffusion coefficient
COPD = chronic obstructive pulmonary disease
DL_{CO} = diffusing capacity for carbon monoxide
FEV_1 = forced expiratory volume in 1 second
FEV_1/FVC = FEV_1 normalized to the forced vital capacity
GOLD = Global initiative for Chronic Obstructuve Lung Disease
PRM = parametric response map
SOC = spatial overlap coefficient
VDP = ventilation defect percent

Author contributions:
Guarantor of integrity of entire study, G.P.; study concepts/study design or data acquisition or data analysis/interpretation, all authors; manuscript drafting or manuscript revision for important intellectual content, all authors; approval of final version of submitted manuscript, all authors; agrees to ensure any questions related to the work are appropriately resolved, all authors; literature research, D.P.I.C., N.Z., F.G., D.P., M.K., G.P.; clinical studies, D.P.I.C., D.G.M., G.P.; experimental studies, D.P.I.C., N.Z., F.G., D.G.M.; statistical analysis, D.P.I.C., F.G., D.P., M.K., G.P.; and manuscript editing, D.P.I.C., N.Z., D.P., M.K., G.P.

Conflicts of interest are listed at the end of this article.

and unpredictable global quantities and high cost have hampered clinical translation. We wanted to determine the quantitative and spatial relationships of PRM gas trapping and PRM emphysema measurements with MR imaging measurements of parenchymal tissue integrity (ie, ADC) and ventilation because these are clinically important imaging findings and phenotypes of COPD. Thus, our objective was to directly compare MR imaging and CT PRM measurements of gas trapping and emphysema in ex-smokers with and without COPD.

Materials and Methods

Study Volunteers

Participants provided written informed consent to a protocol that was approved by a local research ethics board and Health Canada and that was compliant with the Health Insurance Portability and Accountability Act (Institutional Review Board Reg.#00000940). The study was prospectively planned and performed from March 2014 to December 2014.

MR Imaging

Acquisition of conventional proton (hydrogen 1 [^{1}H]), ^{3}He static ventilation, and ^{3}He diffusion-weighted MR images was performed with a whole-body 3-T Discovery MR750 system (GE Healthcare, Milwaukee, Wis), as was previously described (24). Polarization (Polarean; HeliSpin, Durham, NC) was achieved to 40%, and the magnetized gas was diluted with medical-grade nitrogen 2 (N_2) gas to a level of 5 mL per kilogram of body weight. Coronal images (multisection, with no gaps) were acquired with breath holding from functional residual capacity after subjects inhaled a 1-L gas mixture (helium 4 and N_2 for ^{1}H MR imaging and ^{3}He and N_2 for ^{3}He MR imaging). Hydrogen 1 MR imaging was performed with a whole-body radiofrequency coil and a fast spoiled gradient-recalled-echo sequence with a partial echo and the following parameters: total acquisition time, 12 sec; repetition time msec/echo time msec, 4.3/1.0; flip angle, 30°; field of view, 40 × 40 cm; matrix, 128 × 80 (zero padded to 128 × 128); partial-echo percent, 62.5%; bandwidth, 62.50 kHz; one excitation; 14 sections; section thickness, 15 mm; zero gap.

^{3}He static ventilation MR images were acquired by using a fast spoiled gradient-recalled-echo method with a partial echo and the following parameters: total acquisition time, 10 sec; 3.8/1.0; flip angle, 7°; field of view, 40 × 40 cm; matrix, 128 × 80 (zero-padded to 128 × 128); partial-echo percent, 62.5%; bandwidth, 62.50 kHz; one excitation; 14 sections; section thickness, 15 mm; zero gap. ^{3}He diffusion-weighted MR images were also acquired by using fast spoiled gradient-recalled-echo sequence with centric k-space sampling and the following parameters: total acquisition time, 14 sec; 6.8/4.5; flip angle, 8°; field of view, 40 × 40 cm; matrix, 128 × 128; bandwidth, 62.50 kHz; one excitation; seven sections; section thickness, 30 mm; zero gap. Two interleaved images were also acquired, both with and without additional diffusion sensitization and the following parameters: 1.94 G/cm; b = 1.6 sec/cm^2; rise and fall time, 0.5 msec; gradient duration, 0.46 msec; diffusion time, 1.46 msec.

CT Imaging

As was previously described, CT images were acquired with subjects in the supine position approximately 10 minutes before MR imaging and 1 hour after administration of salbutamol. A 64-section Lightspeed VCT imager (GE Healthcare, Milwaukee, Wis) was used to acquire breath-hold images at full inspiration and full expiration by using a spiral acquisition approach and the following parameters: detector configuration, 64 × 0.625 mm; peak voltage, 120 kVp; effective current, 100 mA; rotation time, 500 msec; pitch, 1.0; section thickness, 1.25 mm; number of sections, 200–250, depending on patient size; matrix, 512 × 512 (25). CT data were reconstructed by using a standard convolution kernel to 1.25 mm. The ImPACT CT patient dosimetry calculator *(http://www.impactscan.org/ctdosimetry.htm)*, which is based on the United Kingdom Health Protection Agency NRPB-SR250, and our manufacturer settings were used to calculate total effective dose (1.8 mSv for inspiration and 1.4 mSv for expiration). For inspiration CT, size-specific dose estimate was calculated to be 5–9 mGy on the basis of volumetric CT dose index of 4.4 mGy, total effective dose of 1.8 mSv, and size-dependent conversion factor of 1.00–2.00, an approach used by Christener et al (26,27). For expiration CT, the size-specific dose estimate was 3–7 mGy on the basis of volumetric CT dose index of 3.3 mGy, total effective dose of 1.4 mSv, and size-dependent conversion factor of 1.00–2.00.

MR Image Analysis

As was previously described, ^{3}He MR imaging semiautomated segmentation was performed by a single observer (D.P., with 3 years of experience) to generate ventilation defect percent (VDP), with the ventilation defect volume normalized to ^{1}H MR imaging thoracic cavity volume (28). A detailed description of this process is provided in Appendix E1(online).

CT Image Analysis

CT images were analyzed with Pulmonary Workstation 2.0 (VIDA Diagnostics, Coralville, IA) by a single observer (D.P.I.C.,with 2 years of experience) to measure wall area percent and segment the lung regions. These analyses are fully automated, as was previously described and validated (29,30). The relative area of the CT attenuation histogram of less than −950 HU and −856 HU at inspiratory and expiratory CT, respectively, were determined by using MATLAB (Mathworks, Natick, Mass).

Briefly, pulmonary PRM results can be generated by coregistering inspiratory and expiratory CT images and classifying voxels on the basis of their specific thresholds into healthy, gas-trapping, or emphysema tissue components. The specific details of this process are given in Appendix E1 (online).

Statistics

Analysis of variance was performed with post hoc analysis and Tukey correction to determine differences in

Table 1

Subject Demographics

Characteristic	Healthy Ex-Smokers ($n = 26$)	Ex-smokers with COPD				*P* Value
		All ($n = 32$)	GOLD I ($n = 12$)	GOLD II ($n = 13$)	GOLD III/IV ($n = 7$)	
Age (y)	70 ± 11	74 ± 7	75 ± 8	74 ± 8	73 ± 6	.104
No. of male subjects	15	25	11	9	5	…
Body mass index (kg/m^2)	30 ± 4	26 ± 3	26 ± 3	27 ± 3	26 ± 4	<.001
Smoking history (pack-years)	28 ± 16	43 ± 26	31 ± 17	50 ± 28	51 ± 30	.012
FEV_1*	103 ± 19	73 ± 27	101 ± 14	64 ± 10	39 ± 7	<.001
FEV_1/FVC (%)	80 ± 7	55 ± 11	63 ± 4	55 ± 8	40 ± 5	<.001
Total lung capacity*	96 ± 13	110 ± 16†	103 ± 34‡	106 ± 17	115 ± 20	<.001
Inspiratory capacity*	103 ± 23	91 ± 27	100 ± 23	94 ± 32	70 ± 10	.078
Residual volume*	100 ± 21	140 ± 39	123 ± 16	134 ± 33	180 ± 53	<.001
DL_{CO}*	89 ± 18§	68 ± 23†	73 ± 29‡	66 ± 24	51 ± 15	<.001

Note.—Unless otherwise indicated, data are mean plus or minus standard deviation. *P* values were determined by analysis of variance with Tukey correction.

* Percent of predicted value.

† $n = 31$.

‡ $n = 11$.

§ $n = 25$.

participant characteristics and imaging measurements by using SPSS Statistics V22.0 (SPSS, Chicago, Ill). Pearson correlation coefficients were determined for MR imaging, and PRM measurements were adjusted with Holm-Bonferroni correction. The agreement between CT PRM and ^{3}He MR imaging measurements was evaluated with the Bland-Altman method and GraphPad Prism V6.0 (GraphPad Software, La Jolla, Calif). Multivariate regression models for both PRM gas trapping and PRM emphysema were determined with the step-wise method; variables were added to the model when $P < .15$ and removed when $P \geq .15$ by using SPSS software.

Results

Participant Characteristics

Table 1 shows demographic characteristics and pulmonary function measurements for 58 participants (mean age, 73 years ± 9), including 26 ex-smokers with normal spirometry results (mean age, 70 years ± 11) and 32 ex-smokers with COPD (mean age, 74 years ± 7). Patient subgroups were significantly different with respect to body mass index ($P < .001$), smoking history (pack-years, $P = .01$), forced expiratory volume in 1 second (FEV_1, $P < .001$), FEV_1 normalized to the forced vital capacity (FEV_1/FVC, $P < .001$), and diffusing capacity for carbon monoxide (DL_{CO}, $P < .001$), but not age ($P = .1$).

Qualitative Ventilation and PRM Results

Figure 1 shows MR and CT images in a representative ex-smoker with no airflow limitation and three ex-smokers with COPD. In the two ex-smokers with more advanced COPD (an 84-year-old man with Global Initiative for Chronic Obstructive Lung Disease [GOLD] grade II; FEV_1, 52% of predicted value; FEV_1/FVC, 44%; and a 67-year-old woman with GOLD III disease; FEV_1, 33% of predicted value; FEV_1/FVC, 39%), more pronounced ^{3}He ventilation defects; a greater number of PRM voxels, a finding reflective of emphysema; and elevated ADC values were present. Alternatively, in two ex-smokers with mild or no disease (a 55-year-old man with FEV_1, 83% of predicted value and FEV_1/FVC, 77% and a 69-year-old man with GOLD I disease; FEV_1, 89% of predicted value; FEV_1/FVC, 69%), more homogeneous ventilation and a greater number of PRM voxels were present, findings reflective of normal or healthy tissue.

Ventilation and PRM Measurements by GOLD Severity

Table 2 summarizes the measurements for MR imaging ventilation and emphysema and for CT-derived gas trapping, emphysema, and PRM measurements. In ex-smokers with COPD, VDP ($P < .001$), ADC ($P < .001$), relative area of the CT attenuation histogram of less than −950 HU ($P < .001$), PRM gas trapping ($P < .001$), and emphysema ($P < .001$) were significantly greater than in ex-smokers with no airflow limitation. There were no significant differences in CT airway measurement of wall area percent ($P = .9$). Figure 2 shows that VDP was significantly different between healthy ex-smokers (8% ± 4) and ex-smokers with moderate (GOLD II, 20% ± 11, $P < .001$) to severe (GOLD III/IV, 37% ± 9, $P < .001$) COPD, but not in ex-smokers with mild COPD (GOLD I, 11% ± 6, $P = .5$). VDP was also significantly different between those with GOLD I and GOLD II disease ($P = .04$), those with GOLD II and GOLD II/IV disease ($P < .001$), and those with GOLD I and GOLD III/IV disease ($P < .001$). PRM measurements were significantly different for healthy ex-smokers

Figure 1

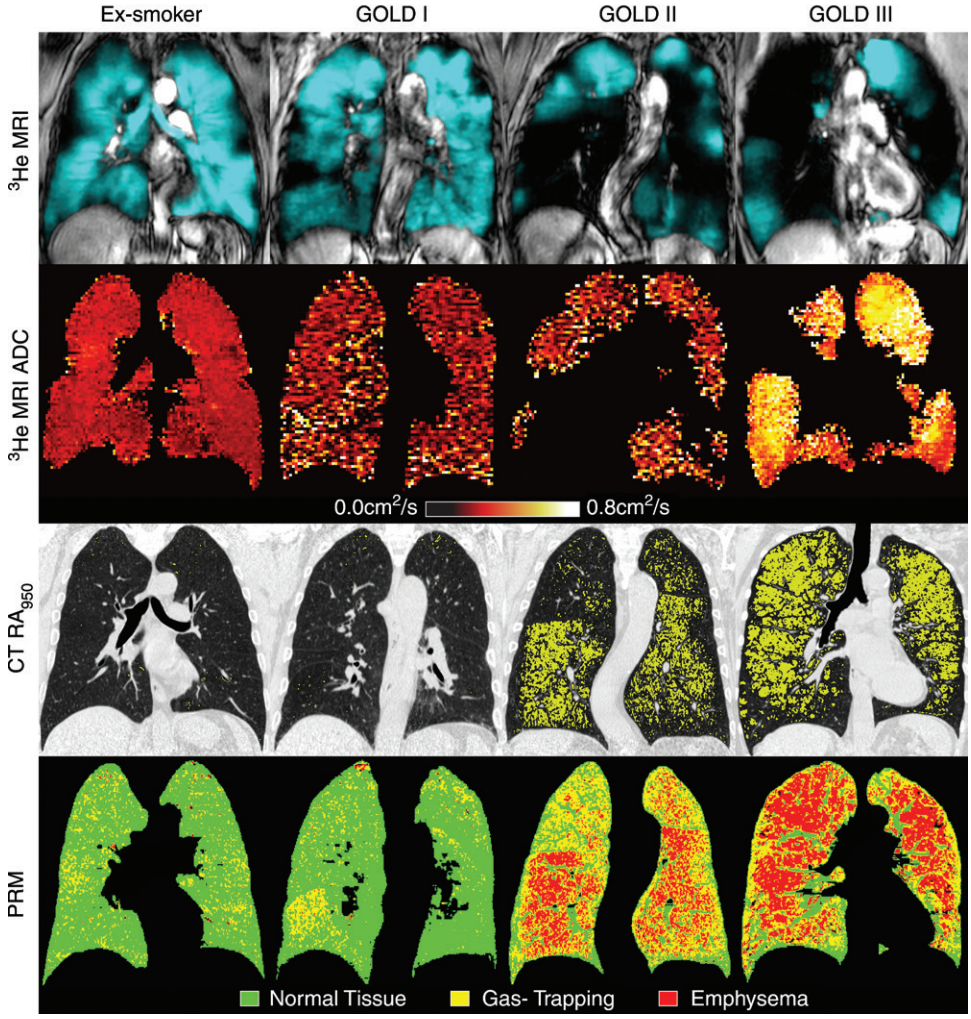

Figure 1: Ventilation and PRM in a 55-year-old man without COPD (FEV_1, 83% of predicted value; FEV_1/FVC, 77%; residual volume to total lung capacity ratio [RV/TLC], 45%), a 69-year-old man with GOLD I disease (FEV_1, 89% of predicted value; FEV_1/FVC, 69%; RV/TLC, 39%; DL_{CO}, 67% of predicted value), an 84-year-old man with GOLD II disease (FEV_1, 52% of predicted value; FEV_1/FVC, 44%; RV/TLC, 62%; DL_{CO}, 47% of predicted value), and a 67-year-old woman with GOLD III disease (FEV_1, 33% of predicted value; FEV_1/FVC, 39%; RV/TLC, 72%; DL_{CO}, 28% of predicted value). First row: ^{3}He MR images coregistered with ^{1}H MR images (grayscale) show static ventilation (blue areas). Second row: ^{3}He MR imaging ADC maps show that the ex-smokers with more advanced COPD (GOLD II/III disease) have elevated ADC values. Third row: CT attenuation masks show areas of less than −950 HU (yellow areas). Fourth row: PRMs show areas of healthy tissue (green), gas trapping (yellow), and emphysema (red).

(gas trapping, 13% ± 10; emphysema, 0.5% ± 0.5) and those with moderate (GOLD II: gas trapping, 27 ± 14%, P = .003; emphysema, 8 ± 11%, P = .003) to severe (GOLD III/IV: gas trapping, 41 ± 8%, P < .001; emphysema, 13 ± 12%, P < .001) COPD. PRM gas trapping was significantly different between ex-smokers and those with mild COPD (GOLD I, 31% ± 11, P < .001). PRM emphysema was significantly different between those with GOLD I and GOLD III/IV disease (P = .03). ADC values were significantly different between healthy ex-smokers (0.29 cm^2/s ± 0.08) and those with GOLD II (0.36 cm^2/s ± 0.06, P = .02) and GOLD III/IV (0.41 ± 0.05 cm^2/s, P < .001) disease, but not those with GOLD I disease (0.34 cm^2/s ± 0.03, P = .2).

Relationships for MR Imaging and PRM Measurements

Tables 3 and 4 show the Holm-Bonferroni-corrected Pearson correlations and multivariate regression model results for CT-derived PRM gas trapping and

Table 2

Imaging Measurements

Measurement	Healthy Ex-Smokers (n = 26)	Ex-smokers with COPD				P Value
		All (n = 32)	GOLD I (n = 12)	GOLD II (n = 13)	GOLD III/IV (n = 7)	
CT						
RA_{950} (%)	2 ± 1	10 ± 9	6 ± 4	10 ± 10	15 ± 12	<.001
RA_{856} (%)	14 ± 10	37 ± 18	34 ± 13	35 ± 20	53 ± 16	<.001
6G wall area percent (%)	65 ± 2	65 ± 2	65 ± 2	66 ± 2	66 ± 2	.882
^{3}He MR imaging						
Ventilation (%)	92 ± 4	20 ± 13	88 ± 6	80 ± 11	63 ± 9	<.001
VDP (%)	8 ± 4*	12 ± 4	12 ± 6	20 ± 11	37 ± 9	<.001
ADC (cm^2/sec)	0.29 ± 0.08*	0.36 ± 0.06†	0.34 ± 0.03‡	0.36 ± 0.06§	0.41 ± 0.05	<.001
PRM						
Healthy (%)	85 ± 11	60 ± 18	64 ± 13	63 ± 20	46 ± 17	<.001
Gas trapping (%)	13 ± 10	31 ± 12	31 ± 11	27 ± 14	41 ± 9	<.001
Emphysema (%)	0.5 ± 0.5	7 ± 10	3 ± 3	8 ± 11	13 ± 12	.001

Note.—Data are mean plus or minus standard deviation. P values were determined by analysis of variance with Tukey correction. RA_{950} = relative area of the lung with attenuation values less than −950 HU at inspiration CT, RA_{856} = relative area of the lung with attenuation values less than −856 HU at expiration CT, 6G = sixth-generation airway.

* n = 24.

† n = 30.

‡ n = 11.

§ n = 12.

emphysema measurements. In ex-smokers with COPD only, PRM gas trapping was significantly related to FEV_1/FVC (r = −0.58, P = .003), ADC (r = 0.53, P = .01), and VDP (r = 0.47, P = .03). PRM emphysema was significantly correlated with FEV_1 (r = −0.43, P = .03), FEV_1/FVC (r = −0.52, P = .008), DL_{CO} (r = −0.69, P < .001), ADC (r = 0.69, P < .001), and VDP (r = 0.62, P < .001) in ex-smokers with COPD. Figure 3 shows linear regressions for PRM gas trapping and emphysema and shows that VDP was significantly correlated with PRM gas trapping (r = 0.58, P < .001) and PRM emphysema (r = 0.68, P < .001) in all subjects and in ex-smokers with COPD (gas trapping: r = 0.47, P = .03; emphysema: r = 0.62, P < .001), but not in healthy ex-smokers. ADC was also significantly correlated with PRM gas trapping (r = 0.55, P < .001) and PRM emphysema (r = 0.62, P < .001) in all subjects and in ex-smokers with COPD (gas trapping: r = 0.53, P = .01; emphysema: r = 0.69, P < .001), but not in healthy ex-smokers. Figure 3 also shows Bland-Altman plots for PRM gas trapping and emphysema. In relation to VDP, there was a negative bias for PRM gas trapping (−9% ± 12; 95% confidence interval: −32%,15%) and a positive bias for PRM emphysema (11% ± 9; 95% confidence interval: −6%, 28%). Table 4 shows that, in the multivariate regression model that explains PRM gas trapping, FEV_1/FVC (standardiced coefficient [β_S] = −0.69, P = .001) and wall area percent (β_S = −0.22, P = .02) make significant contributions, whereas, for the PRM emphysema model, DL_{CO} (β_S = −0.29, P = .03) and VDP (β_S = 0.41, P = .001) were significant.

Spatial and Regional Relationships

Given the significant quantitative relationships between MR imaging and PRM COPD measurements, we evaluated the spatial correlations of ventilation defects with PRM measurements. Qualitative examples are shown in Figure 4 for an ex-smoker with mild COPD and another with GOLD III COPD. The spatial relationship between ventilation defects and PRM gas trapping is more obvious in the ex-smoker with mild disease, whereas colocalization of PRM emphysema and ventilation defects are present in the ex-smoker with severe airflow limitation.

To explore these relationships in more detail, we quantitatively evaluated the spatial overlap of PRM gas trapping and emphysema voxels with ADC and ventilation defects (Table 5, Fig 5). As shown in Figure 5, ^{3}He ADC was significantly elevated in areas of PRM gas trapping compared with healthy tissue (P = .004 in a healthy ex-smoker, P = .01 in patients with GOLD I and GOLD II disease, P = .03 in a patient with GOLD III/IV disease). Helium 3 ADC values were also significantly greater in the regions of PRM emphysema compared with regions of PRM gas trapping in patient with GOLD I disease (P = .03), but not in healthy ex-smokers or those with GOLD II, III, or IV disease. Table 5 shows that, in mild and moderate COPD, the MR imaging spatial overlap coefficient (SOC) for ^{3}He ventilation defects with PRM gas trapping tissue (MR imaging SOC = 36% ± 28 and MR imaging SOC = 34% ± 28 in those with mild and moderate disease, respectively) was significantly greater than for PRM emphysema

Figure 2

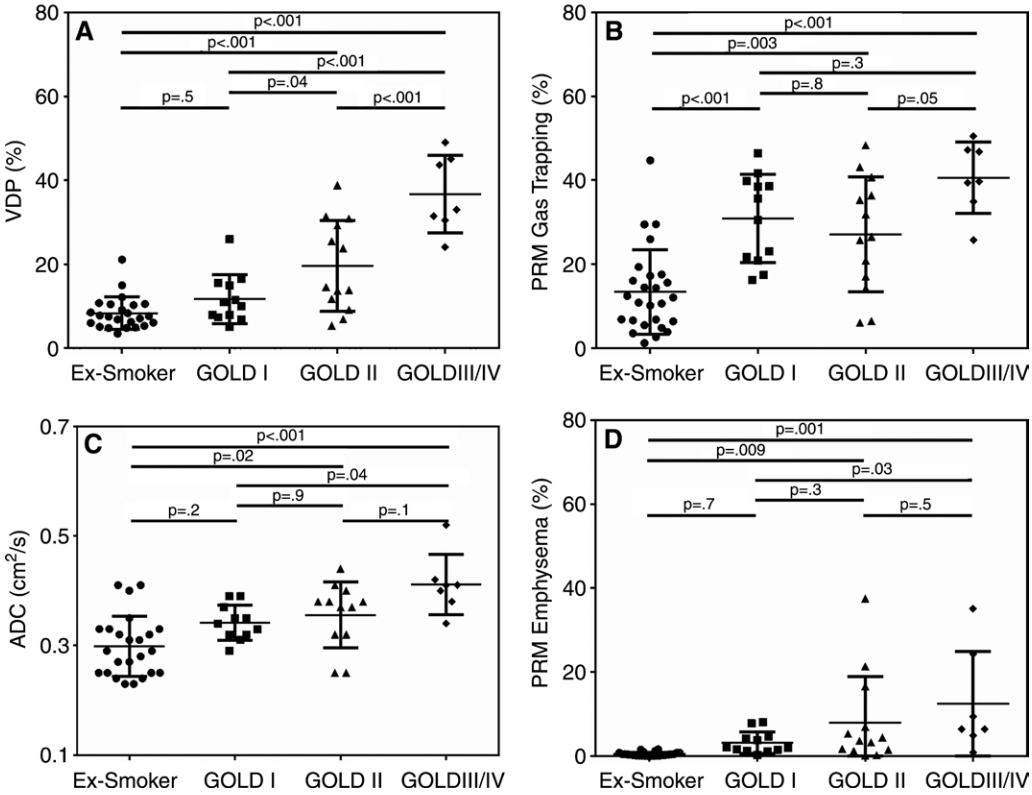

Figure 2: ^{3}He MR imaging ventilation and PRM measurements by COPD grade. *A*, Box plot shows ^{3}He MR imaging VDP in ex-smokers without COPD (8% ± 4) and with GOLD I (11% ± 6), GOLD II (20% ± 11), and GOLD III/IV (37% ± 9) disease. There was a significant difference in VDP between ex-smokers without COPD and those with GOLD II disease ($P < .001$), ex-smokers without COPD and those with GOLD III/IV disease ($P < .001$), those with GOLD I and GOLD II disease ($P = .04$), those with GOLD II and GOLD III/IV disease ($P < .001$), and those with GOLD I and GOLD III/IV disease ($P < .001$). *B,* Box plot shows PRM-derived gas-trapping voxels in ex-smokers without COPD (13% ± 10) and ex-smokers with GOLD I (31% ± 11), GOLD II (27% ± 14), and GOLD III/IV (41% ± 8) disease. There is a significant difference in PRM gas trapping between ex-smokers without COPD and those with GOLD I disease ($P < .001$), ex-smokers without COPD and those with GOLD II disease ($P = .003$), and ex-smokers without COPD and those with GOLD III/IV disease ($P < .001$). *C,* Box plot shows ^{3}He MR imaging ADC values in ex-smokers without COPD (0.29 cm^2/s ± 0.08) and those with GOLD I (0.34 cm^2/s ± 0.03), GOLD II (0.36 cm^2/s ± 0.06), and GOLD III/IV (0.41 cm^2/s ± 0.05) disease. There is a significant difference in ADC values between ex-smokers without COPD and those with GOLD II disease ($P = .02$), ex-smokers without COPD and those with GOLD III/IV disease ($P < .001$), and those with GOLD I and GOLD III/IV disease ($P = .04$). *D,* Box plot shows PRM-derived emphysema voxels in ex-smokers without COPD (0.5% ± 0.5) and those with GOLD I (3% ± 3), GOLD II (8% ± 11), and GOLD III/IV (13% ± 12) disease. There is a significant difference in PRM emphysema between ex-smokers without COPD and those with GOLD II disease ($P = .009$), ex-smokers without COPD and those with GOLD III/IV disease ($P = .001$), and those with GOLD I and GOLD III/IV disease ($P = .03$). Significant differences between subgroups ($P < .05$) were determined with analysis of variance and post hoc Tukey analysis. Error bars = standard deviation.

voxels (mild: MR imaging SOC 1% ± 2, $P = .001$, and MR imaging SOC = 7% ± 15, $P = .006$, in those with mild and moderate disease, respectively). Thus, in patients with mild and moderate COPD, ^{3}He ventilation defects showed a greater spatial relationship with PRM gas trapping versus emphysema voxels. In patients with severe COPD, the CT SOC for ^{3}He ventilation defects with PRM emphysema (CT SOC = 64% ± 30) was significantly greater than that for PRM gas trapping voxels (CT SOC = 36% ± 18; $P = .01$). Therefore, for patients with severe COPD, PRM emphysema was mainly localized within regions of ^{3}He ventilation defects. In addition, in patients with severe COPD, MR imaging SOC for ^{3}He ventilation defects with PRM gas trapping voxels (SOC = 62% ± 25) was significantly greater than that for PRM emphysema (SOC = 11% ± 20, $P = .009$). Hence, in patients with severe COPD, regions of

Table 3

Pearson Correlations for PRM Gas Trapping and Emphysema Measurements

	PRM Gas Trapping				PRM Emphysema			
Variable	Healthy Ex-Smokers*	*P* Value	Ex-Smokers with COPD†	*P* Value	Healthy Ex-Smokers*	*P* Value	Ex-Smokers with COPD†	*P* Value
FEV_1‡	−0.09	.9	−0.29	.1	−0.11	.9	−0.43	.03
FEV_1/FVC (%)	−0.33	.6	−0.58	.003	−0.34	.6	−0.52	.008
DL_{CO}‡	−0.06	.8	−0.36	.09	−0.21	.9	−0.69	<.001
ADC (cm^2/sec)	0.08	.9	0.53	.01	0.30	.8	0.69	<.001
6G (%)	−0.16	.9	−0.44	.07	−0.22	.9	−0.14	.4
VDP (%)	0.13	.9	0.47	.03	0.10	.7	0.62	<.001

Note.—Unless otherwise indicated, data are Pearson correlation coefficients. *P* values were determined with Holm-Bonferroni correction. Data were adjusted for age, sex, height, weight, and smoking history. *P* = .15 indicates a significant difference. 6G = sixth-generation airway wall area percent.

* *n* = 26.

† *n* = 32.

‡ Percent of predicted value.

Table 4

Multivariate Regressions for PRM Gas Trapping and Emphysema Measurements

	PRM Gas Trapping				PRM Emphysema			
Variable	β_U	β_S	Partial R^2	*P* Value	β_U	β_S	Partial R^2	*P* Value
FEV_1*	…	…	…	…	…	…	…	…
FEV_1/FVC (%)	−0.65	−0.69	0.53	.001	…	…	…	…
DL_{CO}*	…	…	…	…	−0.10	−0.29	0.10	.03
ADC (cm^2/sec)	…	…	…	…	…	…	…	…
6G (%)	−1.72	−0.22	0.08	.02	…	…	…	…
VDP (%)	…	…	…	…	0.29	0.41	0.20	.001

Note.—Unless otherwise indicated, data are Pearson correlation coefficients. *P* values were determined with Holm-Bonferroni correction. Data were adjusted for age, sex, height, weight, and smoking history. *P* = .15 indicates a significant difference. *n* = 58. 6G = sixth-generation airway, β_U = unstandardized regression coefficient, β_S = standardized regression coefficient.

* Percent of predicted value.

^{3}He ventilation defects mostly consisted of PRM gas trapping voxels, although there was a mixture of PRM gas trapping and emphysema.

Discussion

We evaluated 58 ex-smokers in the first direct comparison of PRM and MR imaging measurements of COPD. We acquired inspiration and expiration CT images and noble gas MR images within 1 hour and observed the following findings: *(a)* with increasing severity of airflow limitation, PRM gas trapping, PRM emphysema, ADC, and VDP measurements were significantly greater; *(b)* ^{3}He ventilation and PRM measurements were correlated in COPD but not in healthy ex-smokers; *(c)* in a multivariate model that predicted PRM gas trapping, wall area percent and FEV_1/FVC were significant, whereas VDP and DL_{CO} were significant for PRM emphysema; and *(d)* ^{3}He ADC values were significantly elevated in regions of PRM gas trapping, and there were quantitative and spatial correlations for both PRM gas trapping and emphysema with ^{3}He ventilation defects that differed according to COPD severity.

PRMs are used to classify lung tissue on the basis of the presence of pulmonary air, either as a consequence of emphysema and gas trapping from airways disease and/or emphysema (9). We were curious about the potential relationships between PRM and MR imaging phenotypes of COPD, especially because both ventilation defects and PRM gas trapping have been suggested as biomarkers of small airways disease. First, we observed that, with increasing severity of airflow limitation, PRM gas trapping, PRM emphysema, ADC, and VDP measurements were significantly greater. We also noted that ^{3}He VDP and PRM measurements were correlated in ex-smokers with COPD but not in ex-smokers with normal pulmonary function. This finding might be expected because correlations in ex-smokers with mainly normal pulmonary function are statistically difficult to ascertain in small sample sizes, since the range of values for normal lung function is small (31). It

Figure 3

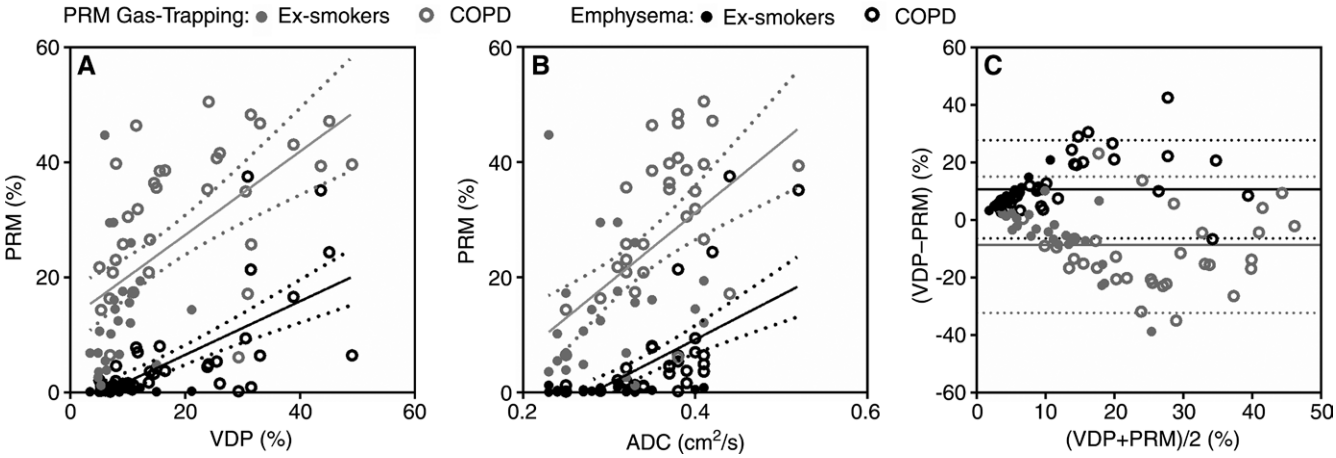

Figure 3: Relationships between ^{3}He MR imaging VDP and ADC with PRM-derived gas-trapping and PRM emphysema voxels. *A,* Scatter plot shows linear regression for ^{3}He MR imaging VDP with PRM in all subjects (gas-trapping voxels: $r = 0.58$, $r^2 = 0.34$, $P < .001$, $y = 0.73x - 12.88$; emphysema voxels: $r = 0.68$, $r^2 = 0.47$, $P < .001$, $y = 0.47x - 2.78$), ex-smokers without COPD (gas-trapping voxels: $r = 0.13$, $r^2 = 0.02$, $P = .9$, $y = 0.35x + 10.92$; emphysema voxels: $r = 0.10$, $r^2 = 0.009$, $P = .7$, $y = 0.01x + 0.39$), and ex-smokers with COPD (gas-trapping voxels: $r = 0.47$, $r^2 = 0.23$, $P = .03$, $y = 0.46x + 22.12$; emphysema voxels: $r = 0.62$, $r^2 = 0.38$, $P < .001$, $y = 0.46x - 2.22$). *B,* Scatter plot shows linear regression for ^{3}He MR imaging ADC with PRM in all subjects (gas-trapping voxels: $r = 0.55$, $r^2 = 0.30$, $P < .001$, $y = 122x - 17$; emphysema voxels: $r = 0.62$, $r^2 = 0.39$, $P < .001$, $y = 77x - 22$), ex-smokers without COPD (gas-trapping voxels: $r = 0.08$, $r^2 = 0.006$, $P = .9$, $y = 14x + 10$; emphysema voxels: $r = 0.30$, $r^2 = 0.09$, $P = .8$, $y = 2.5x - 0.3$), and ex-smokers with COPD (gas-trapping voxels: $r = 0.53$, $r^2 = 0.28$, $P = .01$, $y = 119x - 12$; emphysema voxels: $r = 0.69$, $r^2 = 0.48$, $P < .001$, $y = 121x - 37$). *C,* Bland-Altman plot shows analysis of agreement for ^{3}He MR imaging VDP and PRM in all subjects (gas-trapping voxels: bias = −9% ± 12, lower limit = −32%, upper limit = 15%; emphysema voxels: bias = 11% ± 9, lower limit = −6%, upper limit = 28%), ex-smokers without COPD (gas-trapping voxels: bias = −6% ± 10, lower limit = −26%, upper limit = 15%; emphysema voxels: bias = 8% ± 4, lower limit = 1%, upper limit = 15%), and ex-smokers with COPD (gas-trapping voxels: bias = −11% ± 13, lower limit = −36%, upper limit = 14%; emphysema voxels: bias = 13% ± 10, lower limit = −7%, upper limit = 33%). Dotted lines = 95% confidence intervals.

is also worth noting that, in this study, CT emphysema measurements for healthy ex-smokers were in agreement with previously reported values for healthy subjects (7,32). Importantly, CT may not be adequately sensitive to very mild or subclinical parenchymal and obstructive disease; this may also partially explain the negligible VDP and PRM correlations in healthy ex-smokers (33).

In addition to these bilateral relationships, multivariate modeling identified the parameters that significantly added to the model for PRM gas trapping (wall area percent and FEV_1/FVC) and PRM emphysema (VDP and DL_{CO}). The PRM gas trapping model is intuitive and was developed on the basis of our previous knowledge of the role of airway wall morphologic characteristics in functional small airways disease (34). This finding is also consistent with the major pulmonary imaging and clinical phenotypes that were recently summarized by the Fleischner Society (35). However, we note that, while the significant contribution of DL_{CO} to PRM emphysema is also consistent with a large body of previous work, the contribution of PRM emphysema to ventilation defects is a novel and somewhat surprising result (36). Strong hints that ventilation defects may stem from emphysematous bullae were previously reported in patients with advanced or severe COPD and numerous exacerbations that required hospitalization (22). Together, this information suggests a role for pulmonary imaging to phenotype COPD beyond FEV_1 to help guide therapy and change exacerbations and other outcomes.

These quantitative associations and some obvious qualitative regional relationships led to our exploration of potential spatial correlations. Notably (and unexpectedly), we observed that ^{3}He ADC values were significantly elevated in regions of PRM gas trapping. This surprising result suggested that PRM functional small-airway disease that leads to gas trapping may be seen as enlarged airs paces, which is reflected by elevated ADC values. This is one of the first studies to spatially compare ^{3}He ADC to gas-trapping measurements. This novel finding is in agreement with other studies that demonstrated gravitational and lung volume effects on pulmonary ADC values (39–39). This also suggests that abnormally elevated ADC values may not always reflect emphysematous abnormalities in patients with COPD. There were also spatial correlations in patients with mild and moderate COPD, in whom ^{3}He MR imaging ventilation defects were spatially related to PRM gas trapping. In contrast, in the small group of seven patients with severe COPD, MR imaging ventilation defects were spatially related to both PRM gas trapping and emphysema, which were identified with CT and MR imaging SOC. The rationale for performing SOC analysis in

Figure 4

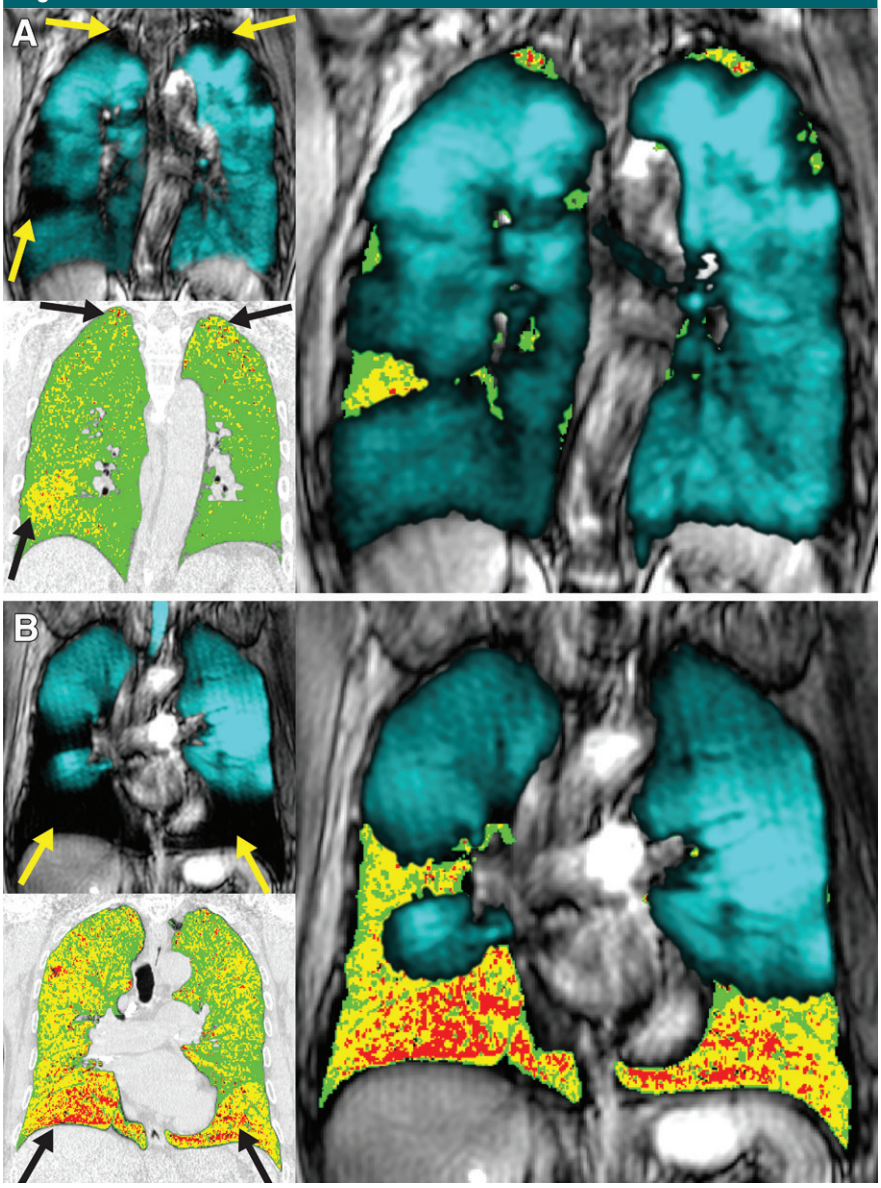

Figure 4: Spatial relationship of ^{3}He MR imaging ventilation defects with PRM gas trapping and emphysema. ^{3}He MR images coregistered with ^{1}H MR imaging and CT obtained in, *A,* a 69-year-old man with mild COPD (GOLD I; FEV_1, 89% of predicted value; FEV_1/FVC, 69%; RV/TLC, 39 FEV_1%, DL_{CO}, 67% of predicted value) and, *B,* a 78-year-old man with severe COPD (GOLD III; 47% of predicted value; FEV_1/FVC, 37%; RV/TLC, 50%; DL_{CO}, 57% of predicted value) show ^{3}He MR imaging ventilation (blue), PRM healthy tissue (green), PRM gas trapping (yellow), and PRM emphysema (red), as well as the spatial relationship between ventilation defects with regions of PRM gas trapping and emphysema (arrows).

both directions was the need to evaluate the overlap of ^{3}He defects within PRM regions (CT SOC) and the overlap of PRM voxels within ^{3}He defects (MR imaging SOC). While the quantitative results showed differences between the two methods, this was not a result of asymmetry between registering from the fixed to the moving image because we performed registration in a symmetric manner to mitigate this potential bias (40,41). It was important to perform the spatial overlap analysis in both directions because the results showed that, in severe COPD, PRM emphysema voxels were mainly occupied by ventilation defect voxels. In contrast, ventilation defect voxels were mainly occupied by PRM gas-trapping voxels. This means that both PRM emphysema and gas-trapping voxels are spatially coincident with ventilation defects. This exciting result provides, for the first time, a deeper understanding of the source of ventilation defects and gas trapping in COPD. We think that these findings underscore the importance of phenotyping COPD cases with quantitative imaging. Future work should aim to determine the spatial relationships between continuous pixel-wise data and PRM, as this may provide a better understanding of these relationships.

Numerous studies have used paired inspiratory and expiratory lung CT images to provide COPD phenotypes (42–44). In patients with COPD, gas trapping is influenced by both emphysema and small-airways disease, differentiation of which is attempted with PRM (43,45). In addition, severe small-airways disease sometimes appears at CT as emphysema, making it challenging to delineate between the two phenotypes. Regardless, in this study, we determined the different relationships between MR imaging and CT phenotypes of COPD cases across GOLD grades of severity. We think that these results underscore the need to adopt multimodality approaches to deeply phenotype COPD cases so that the independent contributions of emphysema and airways disease may be ascertained, which may help optimize COPD therapy and improve outcomes.

In summary, in all ex-smokers, ventilation defects and ADC values were correlated with PRM gas trapping and emphysema measurements. In a subset of ex-smokers with mild to moderate COPD, ventilation defects were quantitatively and spatially related to PRM gas trapping, whereas in severe COPD, there were spatial and quantitative relationships for ventilation defects with both PRM gas trapping and emphysema.

Table 5

Quantitative Spatial Relationships for ^{3}He MR imaging Ventilation Defects with CT PRM Voxels

Characteristic	Healthy Ex-Smokers (n = 26)	Ex-Smokers with COPD				P Value
		All (n = 32)	GOLD I (n = 12)	GOLD II (n = 13)	GOLD III/IV (n = 7)	
Spatial Overlap Coefficient Normalized with CT Voxels						
Gas trapping to VDP (%)	3 ± 12	15 ± 16	4 ± 4	13 ± 13	36 ± 18	<.001
Emphysema to VDP (%)	0 ± 0	22 ± 32	3 ± 9	16 ± 27	64 ± 30	<.001
Significant difference*	0.2	0.06	0.5	0.5	0.01	…
Spatial Overlap Coefficient Normalized with MR Imaging Voxels						
VDP to gas trapping (%)	3 ± 8	41 ± 29	36 ± 28	34 ± 28	62 ± 25	<.001
VDP to emphysema (%)	0 ± 0	6 ± 14	1 ± 2	7 ± 15	11 ± 20	.04
Significant difference*	0.09	<0.001	0.001	0.006	0.009	…

Note.—Unless otherwise indicated, data are mean plus or minus standard deviation. P values were determined with analysis of variance and Tukey correction; $P < .05$ indicates a significant difference.
*Significant difference was measured with paired t test for spatial overlap coefficients of MR imaging ventilation defects with PRM gas trapping and emphysema.

Figure 5

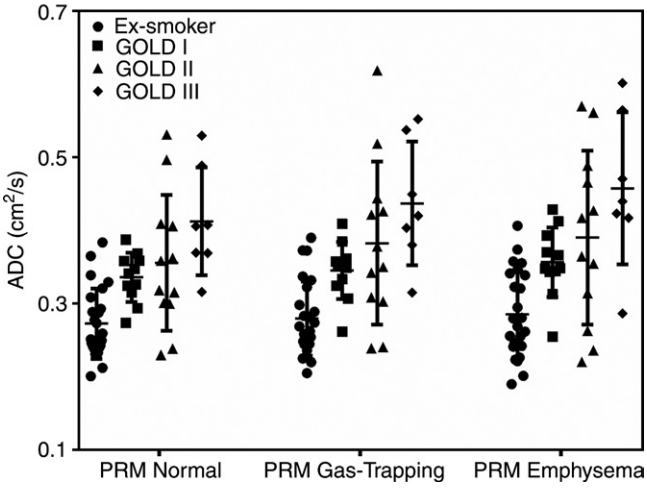

Figure 5: Spatial ^{3}He MR imaging ADC measurements within PRM regions of healthy, gas-trapped, and emphysematous tissue. Box plot shows ^{3}He ADC measurements in PRM regions of healthy tissue (ex-smokers without COPD, 0.27 cm^2/sec ± 0.05 and ex-smokers with GOLD I, 0.34 cm^2/sec ± 0.03; GOLD II, 0.36 cm^2/sec ± 0.09; and GOLD III/IV disease , 0.41 cm^2/sec ± 0.07), gas trapping (ex-smokers without COPD, 0.28 cm^2/sec ± 0.05 and ex-smokers with GOLD II, 0.35 cm^2/sec ± 0.04, GOLD II, 0.38 cm^2/sec ± 0.11; and GOLD III/IV disease, 0.44 cm^2/sec ± 0.08), and emphysema (ex-smokers without COPD, 0.29 cm^2/sec ± 0.06 and ex-smokers with GOLD I, 0.36 cm^2/sec ± 0.05; GOLD II, 0.39 cm^2/sec ± 0.12; and GOLD III/IV disease, 0.46 cm^2/sec ± 0.10). Error bars = standard deviation.

Acknowledgment: We thank Sandra Blamires, CCRC, for clinical coordination and for performing MR imaging of research volunteers.

Disclosures of Conflicts of Interest: **D.P.I.C.** disclosed no relevant relationships. **N.Z.** disclosed no relevant relationships. **F.G.** disclosed no relevant relationships. **D.P.** disclosed no relevant relationships. **D.G.M.** disclosed no relevant relationships. **M.K.** disclosed no relevant relationships. **G.P.** disclosed no relevant relationships.

References

1. Vestbo J, Hurd SS, Agustí AG, et al. Global strategy for the diagnosis, management, and prevention of chronic obstructive pulmonary disease: GOLD executive summary. Am J Respir Crit Care Med 2013;187(4):347–365.
2. Hackx M, Bankier AA, Gevenois PA. Chronic obstructive pulmonary disease: CT quantification of airways disease. Radiology 2012; 265(1):34–48.
3. Nakano Y, Müller NL, King GG, et al. Quantitative assessment of airway remodeling using high-resolution CT. Chest 2002;122(6 Suppl):271S–275S.
4. Hayhurst MD, MacNee W, Flenley DC, et al. Diagnosis of pulmonary emphysema by computerised tomography. Lancet 1984;2(8398): 320–322.
5. Klein JS, Gamsu G, Webb WR, Golden JA, Müller NL. High-resolution CT diagnosis of emphysema in symptomatic patients with normal chest radiographs and isolated low diffusing capacity. Radiology 1992;182(3): 817–821.
6. Dirksen A, Dijkman JH, Madsen F, et al. A randomized clinical trial of alpha(1)-antitrypsin augmentation therapy. Am J Respir Crit Care Med 1999;160(5 Pt 1):1468–1472.
7. Zach JA, Newell JD Jr, Schroeder J, et al. Quantitative computed tomography of the lungs and airways in healthy nonsmoking adults. Invest Radiol 2012;47(10):596–602.
8. Moffat BA, Chenevert TL, Lawrence TS, et al. Functional diffusion map: a noninvasive MRI biomarker for early stratification of clinical brain tumor response. Proc Natl Acad Sci U S A 2005;102(15):5524–5529.
9. Galbán CJ, Han MK, Boes JL, et al. Computed tomography-based biomarker provides unique signature for diagnosis of COPD phenotypes and disease progression. Nat Med 2012;18(11):1711–1715.
10. Cho N, Im SA, Park IA, et al. Breast cancer: early prediction of response to neo-

adjuvant chemotherapy using parametric response maps for MR imaging. Radiology 2014;272(2):385–396.

11. Hoff BA, Kozloff KM, Boes JL, et al. Parametric response mapping of CT images provides early detection of local bone loss in a rat model of osteoporosis. Bone 2012;51(1):78–84.
12. Gevenois PA, de Maertelaer V, De Vuyst P, Zanen J, Yernault JC. Comparison of computed density and macroscopic morphometry in pulmonary emphysema. Am J Respir Crit Care Med 1995;152(2):653–657.
13. Pompe E, van Rikxoort EM, Schmidt M, et al. Parametric response mapping adds value to current computed tomography biomarkers in diagnosing chronic obstructive pulmonary disease. Am J Respir Crit Care Med 2015;191(9):1084–1086.
14. Jögi J, Ekberg M, Jonson B, Bozovic G, Bajc M. Ventilation/perfusion SPECT in chronic obstructive pulmonary disease: an evaluation by reference to symptoms, spirometric lung function and emphysema, as assessed with HRCT. Eur J Nucl Med Mol Imaging 2011;38(7):1344–1352.
15. Brudin LH, Rhodes CG, Valind SO, Buckingham PD, Jones T, Hughes JM. Regional structure-function correlations in chronic obstructive lung disease measured with positron emission tomography. Thorax 1992;47(11):914–921.
16. Kirby M, Mathew L, Wheatley A, Santyr GE, McCormack DG, Parraga G. Chronic obstructive pulmonary disease: longitudinal hyperpolarized (3)He MR imaging. Radiology 2010;256(1):280–289.
17. Kirby M, Svenningsen S, Owrangi A, et al. Hyperpolarized 3He and 129Xe MR imaging in healthy volunteers and patients with chronic obstructive pulmonary disease. Radiology 2012;265(2):600–610.
18. Ohno Y, Iwasawa T, Seo JB, et al. Oxygen-enhanced magnetic resonance imaging versus computed tomography: multicenter study for clinical stage classification of smoking-related chronic obstructive pulmonary disease. Am J Respir Crit Care Med 2008;177(10):1095–1102.
19. Couch MJ, Ball IK, Li T, et al. Inert fluorinated gas MRI: a new pulmonary imaging modality. NMR Biomed 2014;27(12):1525–1534.
20. Fain SB, Panth SR, Evans MD, et al. Early emphysematous changes in asymptomatic smokers: detection with 3He MR imaging. Radiology 2006;239(3):875–883.
21. Swift AJ, Wild JM, Fichele S, et al. Emphysematous changes and normal variation in smokers and COPD patients using diffusion 3He MRI. Eur J Radiol 2005;54(3):352–358.
22. Kirby M, Pike D, Coxson HO, McCormack DG, Parraga G. Hyperpolarized (3)He ventilation defects used to predict pulmonary exacerbations in mild to moderate chronic obstructive pulmonary disease. Radiology 2014;273(3):887–896.
23. Svenningsen S, Kirby M, Starr D, et al. What are ventilation defects in asthma? Thorax 2014;69(1):63–71.
24. Parraga G, Ouriadov A, Evans A, et al. Hyperpolarized 3He ventilation defects and apparent diffusion coefficients in chronic obstructive pulmonary disease: preliminary results at 3.0 Tesla. Invest Radiol 2007;42(6):384–391.
25. Kirby M, Owrangi A, Svenningsen S, et al. On the role of abnormal DL(CO) in exsmokers without airflow limitation: symptoms, exercise capacity and hyperpolarised helium-3 MRI. Thorax 2013;68(8):752–759.
26. Christner JA, Braun NN, Jacobsen MC, Carter RE, Kofler JM, McCollough CH. Size-specific dose estimates for adult patients at CT of the torso. Radiology 2012;265(3):841–847.
27. Brink JA, Morin RL. Size-specific dose estimation for CT: how should it be used and what does it mean? Radiology 2012;265(3):666–668.
28. Kirby M, Heydarian M, Svenningsen S, et al. Hyperpolarized 3He magnetic resonance functional imaging semiautomated segmentation. Acad Radiol 2012;19(2):141–152.
29. Hu S, Hoffman EA, Reinhardt JM. Automatic lung segmentation for accurate quantitation of volumetric X-ray CT images. IEEE Trans Med Imaging 2001;20(6):490–498.
30. Tschirren J, Hoffman EA, McLennan G, Sonka M. Intrathoracic airway trees: segmentation and airway morphology analysis from low-dose CT scans. IEEE Trans Med Imaging 2005;24(12):1529–1539.
31. Sheikh K, Paulin GA, Svenningsen S, et al. Pulmonary ventilation defects in older never-smokers. J Appl Physiol (1985) 2014;117(3):297–306.
32. Schroeder JD, McKenzie AS, Zach JA, et al. Relationships between airflow obstruction and quantitative CT measurements of emphysema, air trapping, and airways in subjects with and without chronic obstructive pulmonary disease. AJR Am J Roentgenol 2013;201(3):W460–W470.
33. Miller RR, Müller NL, Vedal S, Morrison NJ, Staples CA. Limitations of computed tomography in the assessment of emphysema. Am Rev Respir Dis 1989;139(4):980–983.
34. Nakano Y, Wong JC, de Jong PA, et al. The prediction of small airway dimensions using computed tomography. Am J Respir Crit Care Med 2005;171(2):142–146.
35. Lynch DA, Austin JH, Hogg JC, et al. CT-definable subtypes of chronic obstructive pulmonary disease: a statement of the Fleischner Society. Radiology 2015;277(1):192–205.
36. Nambu A, Zach J, Schroeder J, et al. Relationships between diffusing capacity for carbon monoxide (DLCO), and quantitative computed tomography measurements and visual assessment for chronic obstructive pulmonary disease. Eur J Radiol 2015;84(5):980–985.
37. Evans A, McCormack D, Ouriadov A, Etemad-Rezai R, Santyr G, Parraga G. Anatomical distribution of 3He apparent diffusion coefficients in severe chronic obstructive pulmonary disease. J Magn Reson Imaging 2007;26(6):1537–1547.
38. Fichele S, Woodhouse N, Swift AJ, et al. MRI of helium-3 gas in healthy lungs: posture related variations of alveolar size. J Magn Reson Imaging 2004;20(2):331–335.
39. Hajari AJ, Yablonskiy DA, Sukstanskii AL, Quirk JD, Conradi MS, Woods JC. Morphometric changes in the human pulmonary acinus during inflation. J Appl Physiol (1985) 2012;112(6):937–943.
40. Heinrich MP, Jenkinson M, Bhushan M, et al. MIND: modality independent neighbourhood descriptor for multi-modal deformable registration. Med Image Anal 2012;16(7):1423–1435.
41. Modat M, McClelland J, Ourselin S. Lung registration using the NiftyReg package. Medical Image Analysis for the Clinic-A Grand Challenge. 2010; 2010:33–42.
42. Bommart S, Marin G, Bourdin A, et al. Relationship between CT air trapping criteria and lung function in small airway impairment quantification. BMC Pulm Med 2014;14:29.
43. Hersh CP, Washko GR, Estépar RS, et al. Paired inspiratory-expiratory chest CT scans to assess for small airways disease in COPD. Respir Res 2013;14:42.
44. Kim EY, Seo JB, Lee HJ, et al. Detailed analysis of the density change on chest CT of COPD using non-rigid registration of inspiration/expiration CT scans. Eur Radiol 2015;25(2):541–549.
45. Gevenois PA, De Vuyst P, Sy M, et al. Pulmonary emphysema: quantitative CT during expiration. Radiology 1996;199(3):825–829.